Diffuse and Stringy Fibrosis in a Bilayer Interconnected Cable Model of the Left Atrium

Ariane Saliani[1,2], Vincent Jacquemet[1,2]

[1] Université de Montréal, Montreal, Canada
[2] Hôpital du Sacré-Cœur de Montréal

Abstract

Interconnected cable models of cardiac tissue are known for their numerical stability and performance at high resolution, their handling of strong anisotropy and their interpretation as network of resistors. Building such as mesh is however not straightforward. We developed an approach for automatic construction of 3D bilayer interconnected cable models from left atrial geometry and epi- and endocardial fiber orientation fields. The model consisted of a series of longitudinal and transverse cables intertwined like fabric threads, with a spatial discretization of 100 μm. Diffuse fibrosis was introduced as random uncoupling of cell-to-cell longitudinal and transverse connections. Stringy fibrosis was intended to represent collagenous septa and was implemented as a random set of longitudinal lines of transverse uncoupling (along cables) with Poisson-distributed length. The range of possible uncoupling percentages was assessed by investigating the percolation limit. This modeling approach was tested by simulating activation maps in normal and fibrotic tissues.

1. Introduction

Fibrosis extent is a hallmark of the progression of atrial fibrillation. Its spatial distribution may be diffuse, patchy, stringy, or a combination of them [1]. Computer models of the atria incorporating fibrosis have been developed [2]. While microstructure can be easily introduced in 2D models [3,4], the stringy form of fibrosis is notably difficult to implement in cubic or hexahedral meshes, which prompted the design of meshes that align with fiber orientation. Interconnected cable models offer a promising avenue, combining computational speed, numerical stability and flexibility altering conduction properties and handling strong anisotropy [5]. Their use has however been limited by the difficulty to generate such mesh.

In this paper, we present an approach for automatically creating an interconnected cable model of the left atrium in which diffuse and stringy fibrosis can be implemented.

2. Methods

2.1. A cable model of the left atrium

A bilayer interconnected cable model was created from a triangulated surface of the left atrium, epi- and endocardial fiber orientation (Fig. 1A), and resolution Δx. The two layers (epi and endo) were built separately and then coupled.

In each layer, evenly-separated streamlines were traced to represent the vector field of fiber orientation using our previously-published approach [6]. This algorithm ensured that the distance between neighboring streamlines was at least a separation distance d_{sep} and at most $2\,d_{\mathrm{sep}}$. The parameter d_{sep} was heuristically set to $0.745\,\Delta x$. The same process was applied to the vector field orthogonal to fiber orientation, possibly with another value for d_{sep}, leading to different longitudinal and transverse space steps. This generated two orthogonal sets of surface curves (longitudinal and transverse).

The nodes of the cable model were defined as the points of intersection between longitudinal and transverse streamlines. A cable was defined as an ordered sequence of nodes along a longitudinal or transverse streamline. These cables determined the connectivity between the nodes. As a clean-up step, loose ends of cables were eliminated by recursively removing nodes that had only one nearest neighbor. When the extremities of two cables with the same orientation were close enough (within about Δx), merging of these cables was considered, provided that the new connecting edge did not cross any other existing cable. Although this merging operation sometimes broke the d_{sep} constraint, it improved connectivity and increased average cable length.

Within a layer, each node was guaranteed to have between 2 and 4 nearest neighbors that can be classified as next, previous, right or left neighbor relative to the cable, similarly to a square lattice except that one or two neighbors may be missing. Longitudinal and transverse cables created a tessellation of the atrial surface with facets composed of quadrilaterals (vast majority), pentagons (usually

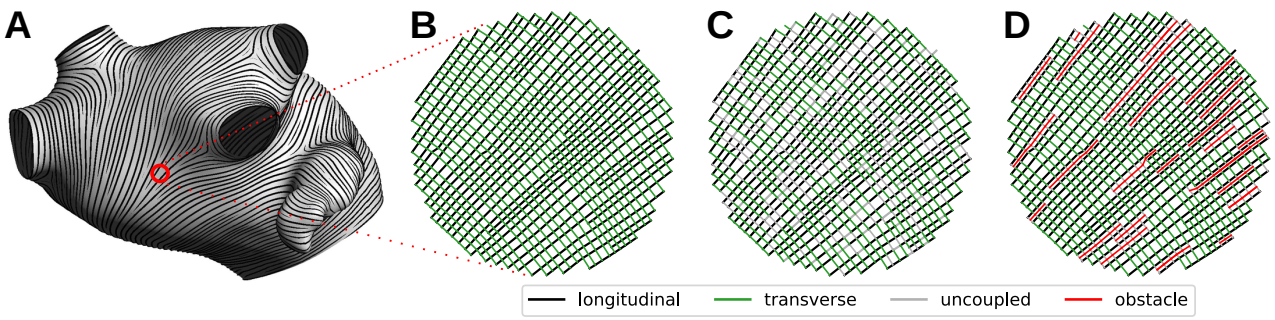

Figure 1. (A) Left atrial geometry with fiber orientation (epicardium). (B) Mesh of the cable model in control. (C) Diffuse fibrosis: 10% longitudinal, 30% transverse. (D) Stringy fibrosis: 20% coverage, $L = 800$ μm.

needed at the extremities of a cable), and some polygons with more vertices (typically found near abrupt changes in fiber orientation). Triangulation of these polygons was used for visualization.

The two layers were connected by identifying the mutual nearest neighbors (i.e., pairs of nodes that were each other's nearest neighbor) between the epi- and endocardial layers. Each node was therefore connected to at most one node from the other layer. For the purpose of specifying coupling conductance, the length of the connection was set to $(d^2 + \Delta x^2)^{1/2}$, where d is the distance on the atrial surface between the mutual nearest neighbors.

With input parameter $\Delta x = 100$ μm, the model was composed of 6920 longitudinal and 8626 transverse cables (mean length: 253 nodes), for a total of 1.96 million nodes. Intra-layer edge length was 101 ± 21 μm, with 1st and 99th percentiles of 70 and 148 μm. Inter-layer edge length was 106 ± 4 μm. In the tessellation, 98.8% of the polygons were quadrilaterals, 1.16% were pentagons, and 0.037% had more vertices. About 76% of the nodes (uniformly distributed over the atrial surface) had an inter-layer (transmural) connection. As a result, the average number of nearest neighbors was 4.75 (including 3.98 intra-layer neighbors).

2.2. Specification of conduction properties

The cable model formed a network of resistors. Each pair of nodes i and j connected by an edge (i, j) were assigned a coupling conductance g_{ij}. To facilitate comparison with continuous models, that conductance was written as $g_{ij} = \beta^{-1}\sigma_{ij}/\ell_{ij}$ where β is the membrane surface-to-volume ratio and ℓ_{ij} is the length of the edge (i, j).

In the baseline model, σ_{ij} was set to σ_l, σ_t or σ_{tm} depending if the edge (i, j) was longitudinal, transverse or transmural (Fig. 1B). In the thin wall limit, reducing transmural conductivity is equivalent to increasing wall thickness [7], which provides a way to partially compensate for the lack of true thickness in a bilayer model.

Diffuse fibrosis was simply simulated by randomly setting coupling conductances to zero (Fig. 1C). Stringy fibrosis generation, on the other hand, exploited the structure of the cable model. Separately in each layer, a set of linear obstacles aligned in the longitudinal direction and uncoupling transverse connections were iteratively generated (Fig. 1D). The fibrosis distribution was characterized by the average length L of obstacles and the fraction f of decoupled connections. First, obstacle length (in number of nodes) was randomly drawn according to a Poisson distribution with mean $L/\Delta x$. A cable was then randomly selected. The obstacle was placed at a random location along that cable. Finally, transverse connections were removed either on the right or on the left of the cable. The process ended when the desired percentage of uncoupling was reached.

2.3. Numerical methods

The cable structure created a natural spatial discretization for the monodomain equation. Reaction and diffusion were separated using second order Strang operator splitting with a time step of 100 μs. Membrane kinetics was described by the Courtemanche model. The reaction step was solved with adaptive time steps of 12.5 μs (depolarization) and 100 μs (repolarization). Each diffusion half-step of the Strang splitting (50 μs) was further separated into longitudinal, transverse and transmural diffusion using first-order splitting, and solved using backward Euler implicit scheme. The advantage of this approach is that the diffusion in each cable is computed independently:

$$C_i \frac{\mathrm{dV_i}}{\mathrm{dt}} = g_{i,\mathrm{prev(i)}}(V_{\mathrm{prev(i)}} - V_i) \quad (1)$$

$$+ g_{i,\mathrm{next(i)}}(V_{\mathrm{next(i)}} - V_i) \quad (2)$$

$$C_i = C_m \frac{\ell_{i,\mathrm{prev(i)}} + \ell_{i,\mathrm{next(i)}}}{2} \quad (3)$$

where V_i is the membrane potential of node i, C_m is the membrane capacitance, and $\mathrm{next(i)}$ and $\mathrm{prev(i)}$ are the

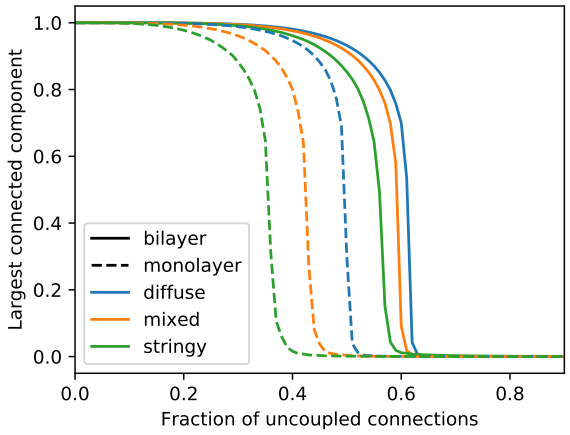

Figure 2. Relative size of the largest connected component of the mesh after uncoupling caused by fibrosis ($L = 1.5$ mm; 90 values of f; $s = 0$, $1/2$ or 1). Lines are colored by fibrosis type. Line type (solid/dashed) denotes the number of layers.

next and previous nodes along the cable. For the first node of the cable, $C_i = C_m \ell_{i,\mathrm{next(i)}}$ and at the other extremity $C_i = C_m \ell_{i,\mathrm{prev(i)}}$. Thus, the cables in each group (longitudinal, transverse and transmural) may be solved in parallel. In the transmural direction (equivalent to a cable of length 2), diffusion was solved analytically. The mathematical formulation was derived so that propagation in a cable network matched the conduction velocities of standard methods in the 1D and 2D cases.

This formulation is amenable to very efficient implementation. As compared to a square regular 2D grid with the same number of nodes and similar discretization, the bilayer cable model was only 15–20% slower and required 20% more memory. The monolayer cable model (epicardium) was only 5% slower than 2D.

2.4. Simulation protocol

Normal and abnormal propagation was simulated in the left atrium by injecting current in the approximate location of the Bachmann's bundle. In the baseline model, the conductivities were set to $\sigma_l = 9$ mS/cm, $\sigma_t = 3$ mS/cm, and $\sigma_{tm} = 1$ mS/cm. Activation maps were computed.

The fibrotic patterns were defined by three parameters: the fraction f of uncoupled connections ($f \leq 40\%$), the fibrosis type (s ranging from 0 to 1) and the mean obstacle length L (ranging from 0.5 to 1.5 mm). A fraction f of the longitudinal and transmural connections were uncoupled. In the transverse direction, stringy fibrosis covering a fraction $s \cdot f$ of the connections was introduced. Among the remaining transverse connections, a fraction $(1-s) \cdot f$ was further removed such that in total a fraction f of the transverse connections were uncoupled. The fibrosis type was called diffuse ($s = 0$), mixed ($s = 1/2$) or stringy ($s = 1$).

The percolation property of fibrosis distributions was assessed by determining the largest connected component of the mesh with uncoupled connections removed (its size being expressed as a fraction of the number of nodes). This is much faster than simulating propagation and does not depend of stimulus location.

3. Results

Figure 2 shows how increasing percentage of uncoupled connections created pieces of isolated tissue. The curves are an average over 10 realizations of the random fibrosis generation process. Up to 40% of uncoupled connections, less than 5% of the tissue was electrically isolated. A transition occurred at about 60% (lower for stringy than diffuse fibrosis), where propagation became no more possible. In a monolayer tissue, that transition was observed earlier due to the lack of zig-zag pathways between layers.

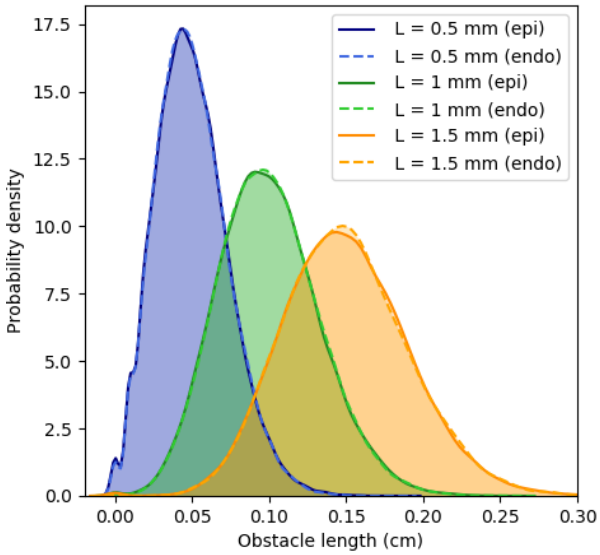

Figure 3. Kernel-based estimate of the probability density of obstacle length for epi and endo layers and three values of L. The length of one-connection long obstacles is zero.

Obstacle length in stringy fibrosis may be expressed as $n \cdot \ell$, where n is the number of segments (mean and variance: $L/\Delta x$) and ℓ is the length of the segment (mean: Δx). Assuming independence, the average obstacle length should be L. Random generation of stringy fibrosis patterns in epi- and endocardial layers with L ranging from 0.1 to 2 mm showed that the expected mean was indeed close to L with a root mean square error of 2 μm, which is much smaller than Δx. Examples of distributions are shown in Fig. 3. The variance of the distribution may be

written as (variance of product formula):

$$\begin{aligned}\mathsf{var}(\mathsf{n}\cdot\ell) &= \mathsf{E}(\mathsf{n})^2\mathsf{var}(\ell) + \mathsf{var}(\mathsf{n})\left(\mathsf{var}(\ell) + \mathsf{E}(\ell)^2\right) \\ &= aL^2 + bL \end{aligned} \quad (4)$$

where $a = 1.5 \times 10^{-3}$ and $b = 108$ μm are fitted parameters that depend on Δx. This formula predicts the standard deviation of obstacle length with an error $< 1.6\%$. The term in L^2 stems from the variability in the space step.

Figure 4 presents activation maps in control and with diffuse, stringy and mixed fibrosis (20% of connections uncoupled in all 3 cases). The total activation time was 97 ms (control), 147 ms (diffuse), 153 ms (mixed) and 163 ms (stringy). Isochrones were more irregular in the stringy case.

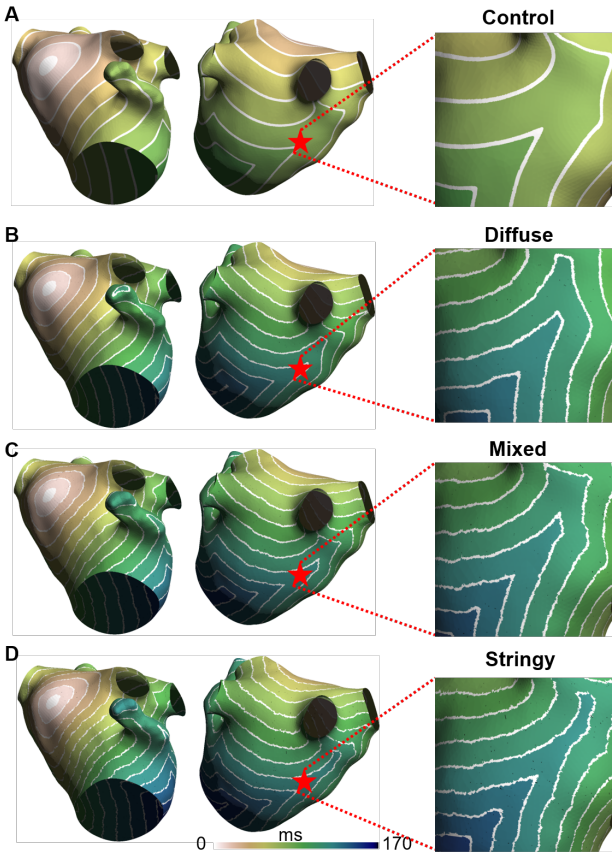

Figure 4. Activation maps. (A) control; (B) diffuse fibrosis; (C) mixed fibrosis; (D) stringy fibrosis.

4. Discussion

We presented a proof of concept for automatic generation of interconnected cable model based on our streamline visualization tools. The resulting model preserves the upsides of Vigmond's model [5] and enables the simulation of propagation in tissue with fibrosis independently specified in the longitudinal and transverse directions. Extension to more layers to better account for tissue thickness is possible. A limitation is reduced efficiency (shorter cables) when fiber orientation is very irregular.

5. Conclusions

While bilayer cable models may be viewed as a simplification of full 3D models, they enable simulations at 100-μm resolution without sacrificing computational speed. These models may bridge the gap between microstructure and the morphology of the atria with little overhead as compared to 2D models.

Acknowledgements

This work was supported by the Natural Sciences and Engineering Research Council of Canada (NSERC grant RGPIN-2020-05252).

References

[1] Kawara T, Derksen R, de Groot JR, Coronel R, Tasseron S, Linnenbank AC, Hauer RN, Kirkels H, Janse MJ, de Bakker JM. Activation delay after premature stimulation in chronically diseased human myocardium relates to the architecture of interstitial fibrosis. Circulation 2001;104(25):3069–3075.

[2] Trayanova NA. Mathematical approaches to understanding and imaging atrial fibrillation: Significance for mechanisms and management. Circ Res 2014;114(9):1516–1531.

[3] Jacquemet V, Henriquez CS. Genesis of complex fractionated atrial electrograms in zones of slow conduction: A computer model of microfibrosis. Heart Rhythm 2009;6(6):803–810.

[4] Nezlobinsky T, Solovyova O, Panfilov AV. Anisotropic conduction in the myocardium due to fibrosis: The effect of texture on wave propagation. Sci Rep 2020;10(1):764.

[5] Vigmond EJ, Ruckdeschel R, Trayanova N. Reentry in a morphologically realistic atrial model. J Cardiovasc Electrophysiol 2001;12(9):1046–1054.

[6] Saliani A, Tsikhanovich A, Jacquemet V. Visualization of interpolated atrial fiber orientation using evenly-spaced streamlines. Comput Biol Med 2019;111:103349.

[7] Labarthe S, Bayer J, Coudière Y, Henry J, Cochet H, Jaïs P, Vigmond E. A bilayer model of human atria: Mathematical background, construction, and assessment. Europace 2014; 16 Suppl 4:iv21–iv29.

Address for correspondence:

Vincent Jacquemet
Hôpital du Sacré-Cœur de Montréal, Centre de Recherche
5400 boul. Gouin Ouest
Montreal (Québec) Canada H4J 1C5
vincent.jacquemet@umontreal.ca